Virus Research 342 (2024) 199337

Contents lists available at ScienceDirect

Virus Research

journal homepage: www.elsevier.com/locate/virusres

Transcriptomics of Marburg virus-infected primary proximal tubular cells reveals negative correlation of immune response and energy metabolism

Benjamin Koch [a,*], Maximilian Filzmayer [b], Sammy Patyna [a], Nils Wetzstein [c], Sebastian Lampe [d], Tobias Schmid [d], Helmut Geiger [a], Patrick C. Baer [a], Olga Dolnik [e,*]

[a] Goethe University Frankfurt, University Hospital, Department of Internal Medicine 4, Nephrology, Theodor-Stern-Kai 7, Frankfurt am Main 60596, Germany
[b] Goethe University Frankfurt, University Hospital, Department of Urology, Frankfurt am Main 60596, Germany
[c] Goethe University Frankfurt, University Hospital, Department of Internal Medicine, Infectious Diseases, Frankfurt am Main 60596, Germany
[d] Goethe University Frankfurt, University Hospital, Faculty of Medicine, Institute for Biochemistry I, Frankfurt am Main 60596, Germany
[e] Philipps University Marburg, Institute of Virology, Hans-Meerwein-Str. 2, Marburg 35043, Germany

ARTICLE INFO

Keywords:
Marburg virus
Human primary proximal tubular cells
Acute kidney injury
PGC-1α

ABSTRACT

Marburg virus, a member of the Filoviridae, is the causative agent of Marburg virus disease (MVD), a hemorrhagic fever with a case fatality rate of up to 90 %. Acute kidney injury is common in MVD and is associated with increased mortality, but its pathogenesis in MVD remains poorly understood. Interestingly, autopsies show the presence of viral proteins in different parts of the nephron, particularly in proximal tubular cells (PTC). These findings suggest a potential role for the virus in the development of MVD-related kidney injury. To shed light on this effect, we infected primary human PTC with Lake Victoria Marburg virus and conducted transcriptomic analysis at multiple time points. Unexpectedly, infection did not induce marked cytopathic effects in primary tubular cells at 20 and 40 h post infection. However, gene expression analysis revealed robust renal viral replication and dysregulation of genes essential for different cellular functions. The gene sets mainly downregulated in PTC were associated with the targets of the transcription factors MYC and E2F, DNA repair, the G2M checkpoint, as well as oxidative phosphorylation. Importantly, the downregulated factors comprise PGC-1α, a well-known factor in acute and chronic kidney injury. By contrast, the most highly upregulated gene sets were those related to the inflammatory response and cholesterol homeostasis. In conclusion, Marburg virus infects and replicates in human primary PTC and induces downregulation of processes known to be relevant for acute kidney injury as well as a strong inflammatory response.

1. Introduction

Marburg virus (MARV) is the causative agent of Marburg virus disease (MVD), a hemorrhagic fever with a case fatality rate of up to 90 %, that is modulated by viral strain, infectious dose, host factors and available medical care (Brauburger et al., 2012; Feldmann et al., 2013; Ligon, 2005). MARV, like Ebola virus, belongs to the Filoviridae. Filoviruses are characterized by a long filiform virion containing a negative-sense, non-segmented RNA genome with seven open reading frames. They encode for the nucleoprotein (NP), virion proteins (VP) 35 and VP40, glycoprotein (GP), VP30, VP24 and viral polymerase L (Dolnik et al., 2008), as well as numerous non-coding RNAs (Prasad et al., 2020). MARV was identified and MVD first described in 1967, when monkey handlers, laboratory- and medical staff in Marburg, Frankfurt and Belgrade were infected by grivets while making primary cultures of kidney cells for polio vaccine production, caring for MVD patients, or conducting causal analysis (Mehedi et al., 2011; Poliquin et al., 2019). However, most common transmissions to humans occur through contact with bodily fluids or flesh from Egyptian fruit bats (Rousettus aegypticus), a natural host of MARV, or through infected wildlife (Amman et al., 2012). After exposure to mucosa or skin lesions, dendritic cells, monocytes, and macrophages represent the primary infected target cells (Martines et al., 2015; Rougeron et al., 2015), disseminating the virus systemically via the lymphoid and vascular route to the internal and reproductive organs (Bente et al., 2009). The initial signs of MVD mimic a feverish acute gastrointestinal illness, accompanied by a pronounced fatigue, often followed by a more-specific maculopapular rash (Brauburger et al., 2012). This stage of MVD can be

* Corresponding authors.
E-mail addresses: b.koch@med.uni-frankfurt.de (B. Koch), dolnik@staff.uni-marburg.de (O. Dolnik).

https://doi.org/10.1016/j.virusres.2024.199337
Received 11 December 2023; Received in revised form 8 February 2024; Accepted 9 February 2024
Available online 13 February 2024

described as a generalization phase, which is followed by an early and late organ stage (or a convalescence phase) (Stille et al., 1971). During the early organ phase abnormal vascular permeability may develop, leading to dyspnea, edema, conjunctival injection, and neurological symptoms (Martini and Siegert, 1971). The late organ phase is defined by a sepsis-like phenotype with dysregulated cytokine release, severe vascular dysfunction, hemorrhage, but also coagulopathy and severe acid-base disturbances, all together often leading to multiple organ failure and death (Martini and Siegert, 1971; Paassen et al., 2012; Poliquin et al., 2019). As for renal damage in MVD, autopsies have shown acute tubular insufficiency with flattened tubular epithelium and degenerated cells, but also tubular necrosis with predominant damage to proximal but not to distal tubular cells (Gear et al., 1975; Gedigk et al., 1968; Rippey et al., 1984). Concomitantly, MARV antigen was revealed in proximal tubular epithelial cells (PTC) as well as glomerular endothelial -and interstitial cells (Zaki and Goldsmith, 1999). Furthermore, MARV has been detected by electron microscopy in human kidney tissue and live virus isolated from it as well as from urine (Martini and Siegert, 1971; Smith et al., 1982).

However, the pathogenesis of acute kidney injury (AKI) in MVD remains poorly understood. Therefore, we performed a comprehensive transcriptome analysis of MARV-infected primary human PTC at multiple time points and uncovered deregulation of several host-cell factors relevant for tubular dysfunction.

2. Materials and methods

2.1. Cells

Proximal tubular epithelial cells (PTC) were isolated from noncancerous kidney tissue after tumour nephrectomy using magnetic cell separation technology as described previously (Baer et al., 1997). Briefly, kidney tissue was minced with crossed blades, digested with collagenase-dispase, and passed through a mesh (106 μm). The cells were then incubated with collagenase IV, DNase and $MgCl_2$ and centrifuged using a Percoll density gradient. Highly purified PTC were then enriched using a monoclonal antibody against aminopeptidase M (CD13, clone SJ1D1, #sc-18,899, Santa Cruz, USA) and the Mini-MACS system (Miltenyi, Germany). Isolated PTC were strongly positive for aminopeptidase M. Ultrastructural analysis revealed well preserved brush border microvilli, a well-developed endocytic apparatus and numerous mitochondria (Baer et al., 2006, 1997). Isolated cells were seeded in cell culture plates and cultured in standard culture medium (Medium 199 (M4530, Sigma, Germany) with 10 % fetal bovine serum (FBS; Biochrom, Germany). The medium was changed every three to four days and confluent cells were passaged by trypsinization. Cells between passages 2 and 5 were used for experiments. Cultured PTC were characterized as described previously (Baer et al., 2006; 1997).

2.2. Virus inoculation

Marburg virus (strain Lake Victoria, Musoke-80) was propagated on VeroE6 cells in presence of 3 % fetal bovine serum and virus stocks stored as cell-debris cleared supernatants at −80 °C. Experiments with MARV were performed under biosafety level 4 (BSL-4) conditions at the Institute of Virology, Philipps-University, Marburg, Germany.

2.3. Infections and sample collection

PTC were plated in 6-well plates at a density of 4×10^5 cells per well. Infections for the transcriptome analysis were carried out with MARV at a multiplicity of infection (MOI) = 1 in a BSL-4 laboratory. Infected PTC were collected in RLT+β-mercaptoethanol buffer (Qiagen, Germany) at 20 h and 40 h post infection (p.i.), mixed with one volume of 70 % ethanol, transferred out of the BSL-4 laboratory and stored at −80 °C until RNAseq library preparation or quantitative real-time PCR (RT-qPCR).

2.4. Transcriptome analysis

Six biological replicates of PTC (cultured in 6-well plates) were either left uninfected or infected with MARV at MOI = 1. Three replicates of each setting were analyzed for transcript expression changes by RNAseq, while the remaining replicates were used to verify RNAseq results by RT-qPCR. Briefly, total RNA was extracted from MARV-infected / uninfected PTC at 20 h and 40 h p.i. using the Qiagen RNeasy Maxi Kit (Qiagen, Germany), including on-column removal of DNA by digestion with rDNase for 15 min at room temperature. Next 1000 ng (each with a RIN score of >9) were used for library preparation. After depletion of ribosomal RNA (NEBNext rRNA Depletion Kit, #E6310, New England Biolabs, Germany), directional libraries were prepared using a NEBNext® UltraTM Directional RNA Library Prep Kit for Illumina® sequencing (#E7420S, New England Biolabs, Germany). Sequencing was performed on an Illumina NextSeq500® using a NextSeq® 500/550 High Output Kit v2 (75 cycles, #FC- 404–2005, Illumina, USA). The total output was 46.6 GBP (approximately 66 million reads per sample). Illumina BCL files were converted to FASTQ by bcl-convert (Illumina, USA), quality controlled by FastQC (Babraham Institute, UK, http://www.bioinformatics.babraham.ac.uk/projects/fastqc/) and Illumina adapters trimmed by Trimmomatic v0.40 (Bolger et al., 2014). Quantification of transcript expression and virus copies was performed by kallisto software (version 0.46.1) (Bray et al., 2016) with standard configurations using a kallisto index build from the hg38 assembly (GRCh38.p12 cDNA) and the NCBI reference sequence from the MARV isolate "Marburg virus/H.sapiens-tc/KEN/1980/Mt. Elgon-Musoke. NC_001608.3", respectively. Differential expression analysis, Principal Component Analysis (PCA), Uniform Manifold Approximation and Projection (UMAP), Kyoto Encyclopedia of Genes and Genomes (KEGG) and Gene Ontology (GO) analyses, as well as volcano plots were done by Omics Playground v.2.8.5 (Akhmedov et al., 2019). Counts per million (CPM) represent average logarithmically transformed counts. UMAP, a manifold learning and dimension reduction algorithm generates a low-dimensional representation of high-dimensional data by learning the data's essential topological structure (McInnes et al., 2018). "Minus over average" (MA) plots and heatmaps were done by the R package iDEP (version 0.96) (Ge et al., 2018). Functional interpretation of large gene lists was done by GO analysis based on known gene product properties. Thereby over-represented biological processes and compartments were investigated. For the latter the "Jensen COMPARTMENT" database (Binder et al., 2014) was utilized via ShinyGO (Ge et al., 2019) (version 0.77) at a false discovery rate (FDR) of 0,05. Network analysis of differentially regulated coding genes using the Ensembl gene set (ENSG) was performed by STRING v11.0 (Mering et al., 2003) (https://string-db.org) using "highest confidence" as the parameter. Next, the network was imported into Cytoscape 3.9.1 (https://cytoscape.org) (Shannon et al., 2003) and the PGC-1α subnetwork extracted with all direct interaction partners. For all analyses the fold change cut-off was set at 2 (log2FC = 1).

2.5. RT-qPCR analysis

Relative expression levels of selected mRNAs were quantified after infection of PTC (MOI = 1). Total RNA was extracted using the RNeasy Maxi Kit (Qiagen, Germany) including on-column removal of DNA by digestion with rDNase for 15 min at room temperature, and cDNA for quantitative real-time RT-PCR (qPCR) was synthesized using 1000 ng RNA in a 15 μl reaction volume. qPCR reactions were set up to a final volume of 20 μl, using the HOT FIREPol EvaGreen qPCR Supermix (Solis Biodyne, Estonia) and primers for ß-actin (FWD 5′-ACTGGAACGGTGAAGGGTGAC-3′, REV 5′-AGAGAAGTGGGGTGGCTTTT-3′) and PGC-1α (FWD 5′-CTGCTAGCAAGTTTGCCTCA-3′, REV 5′- AGTGGTGCAGTGACCAATCA-3′). The qPCR reaction was performed on an ABI PRISM

7900HT Fast Real-Time PCR System with Sequence Detection System SDS 2.4.1 software (both Applied Biosystems, USA), using 40 cycles of the following program: 95 °C for 15 s, 63 °C for 15 s and 72 °C for 20 s (SDS 2.4.1. settings: automatic baseline, threshold 0.2). To exclude artefacts due to primer dimer formation, melting curve analysis was performed using the sequence 95 °C for 15 s, 60 °C for 15 s, 95 °C for 1 min and 37 °C for 30 s. The results shown represent the mean of three independent experiments. Relative expression of the mRNA target was assessed using the ΔΔCt method (Pfaffl, 2001) with β-actin as calibrator, and target gene expression levels were estimated by $2-\Delta\Delta Ct$.

2.6. Statistics

Results are expressed as mean ± standard deviation (SD). Error bars represent the mean± SD of at least three independent experiments. The difference between two mean values was analyzed using Dunnett's Multiple Comparison Test or Student's *t*-test using GraphPad Prism software version 8.0 for OS X (GraphPad Software Inc., USA). The difference was considered statistically significant when $p < 0.05$. For transcriptomics a q-value (Bonferroni-Hochberg adjusted p-value) of <0.05 was employed.

2.7. Biosafety

All experiments with infectious virus were performed according to German regulations for the propagation of filoviruses. All experiments involving Marburg virus were performed in a biosafety level 4 (BSL-4) containment laboratory at the Institute of Virology, Philipps-University, Marburg, Germany approved by the local authorities (RP Giessen, Germany).

3. Results

3.1. Marburg virus can infect and replicate in human kidney cells in vitro

To investigate whether MARV can infect and replicate productively in human PTC, primary isolated PTC were infected with MARV Lake Victoria (Musoke-80) strain. This strain originated from the Mount Elgon cases in Kenya in 1980. Importantly, virus particles were found post-mortem in renal tissue from the index patient, in addition MARV was successfully isolated from a patient experiencing AKI (Smith et al., 1982). We analyzed virus genome copies at multiple timepoints by kallisto and detected high virus abundance in all infected PTC samples (Fig. 1A), with an average of 785,197 copies at 20 h post infection (p.i.) and 1,566,421 copies at 40 h p.i. respectively. Interestingly, an apparent cytopathic effect (CPE) could not be observed at both time points (Fig. 1B).

3.2. Transcriptomics of PTC reveal changes of multiple cellular factors relevant for AKI development

To identify differential gene expression relevant to tubular dysfunction, transcriptomics were performed at 20 h and 40 h p.i. Heatmap and principal component analysis showed a clear separation of gene expression in infected and mock samples at 20 h p.i., but more pronounced at 40 h p.i. (Fig. 1C, E). In total 639 up- and 478 downregulated gene transcripts were identified at 40 h p.i. (q-value ≤ 0.05, fold change (FC) ≥2 (logFC ≥1) (Fig. 1D, Supplemental Table S1). The top up- and downregulated genes are represented in Tables 1, 2 and Fig. 2A.

The most upregulated genes identified, belong to interferon-related factors and cytokines, like RSAD2, OASL, CXCL10, IFNB1 or IFITM2 (Table 1, Fig. 2A). In comparison, the top downregulated genes at 40 h p.i. are led by RPL14, SLC35B2 and MATR3 (Table 2, Fig. 2A).

Other top downregulated factors upon MARV infection of primary PTC are involved in STING activation or cellular energy homeostasis. The SLC35B2 gene codes for the sulfotransferase PABST1, an enzyme necessary for STING activation (Fang et al., 2021). MATRIN3 (MATR3) takes part in RNA processing, the assembly of nuclear paraspeckles (Banerjee et al., 2017) and cGAS-STING activation (Morchikh et al., 2017). DGUOK is an important factor in mitochondrial DNA synthesis, while SLC2A2 codes for GLUT2, a glucose transporter expressed in renal proximal tubular cells, hepatocytes, and the small intestine's enterocytes (Digre and Lindskog, 2020). MC4R is coding for the melanocortin 4 receptor, a central player in energy homeostasis (Krashes et al., 2016). To determine the primary subcellular localizations involved in

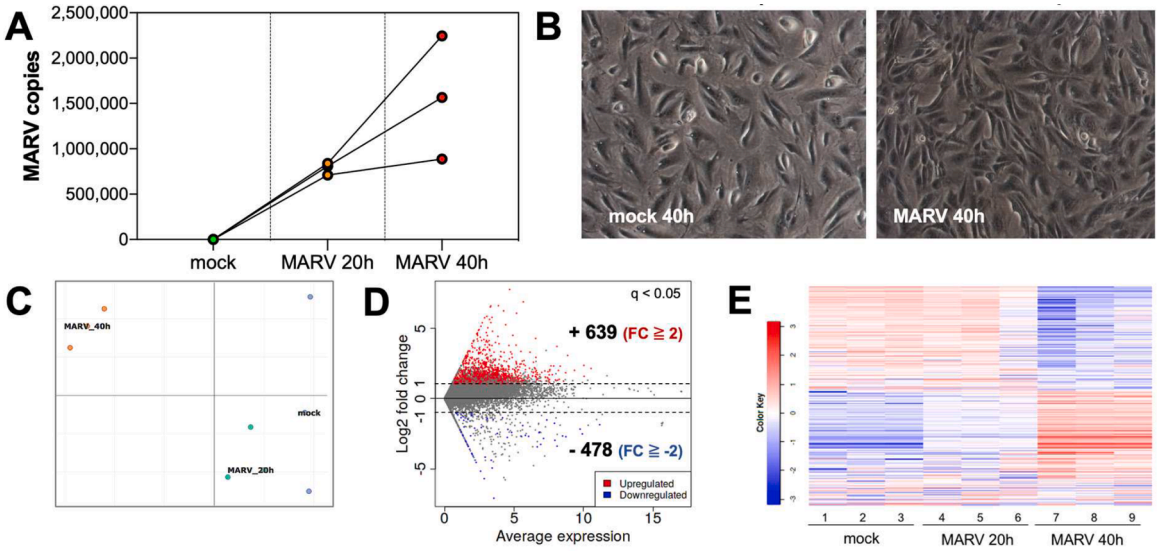

Fig. 1. MARV infection of primary human proximal tubular cells (PTC). (A) MARV copies (by kallisto) at 20 h and 40 h post infection (p.i.). Mock: three uninfected PTC replicates from 40 h p.i. **(B)** Bright field image of mock and MARV infected PTC at 40 h p.i. taken with 10x objective at a NIKON TS-100 microscope. **(C)** Principial component analysis of mock-infected, 20 h- and 40 h MARV-infected PTC, demonstrating a transcriptome difference at 20 h- and especially at 40 h p.i. **(D)** MARV transcriptomics at 40 h p.i.: MA plot, depicting significantly ($q<0.05$) up-regulated transcripts in red and down-regulated ones in blue (cut-off fold-change ≥2). **(E)** Heatmap of gene expression changes after MARV infection, again demonstrating transcriptome differences at 20 h- and especially at 40 h p.i. (replicates: 1–3: mock; 4–6: 20 h p.i. and 7–9: 40 h p.i. The heatmap is color coded: blue represents down- and red upregulated genes).

Table 1
Top 30 upregulated genes after MARV infection of primary PTC (40 h p.i.)(Ave. = average, q-value = FDR adjusted p-value).

Gene	Fold change	q-value	Ave. Mock	Ave. MARV
RSAD2	996.00	2.6E-06	0.0381	9.9945
OASL	709.18	2.7E-06	0.0000	9.4701
CXCL10	613.11	1.7E-05	0.5879	9.8503
IFNB1	372.22	3.4E-06	0.0000	8.5416
IFITM2	330.84	0.0004	0.9297	9.3034
OAS1	257.78	5.9E-05	0.5841	8.5968
IFI6	225.97	0.0256	1.8723	9.6895
IFNL1	210.84	0.0002	0.0000	7.7244
IFNL3	179.77	0.0022	0.0000	7.4912
IFNL2	177.29	0.0004	0.0000	7.4742
AKR1B15	171.25	0.0006	0.0000	7.4188
IFIT2	119.43	2.7E-05	3.7160	10.6114
TNFSF15	100.43	2.6E-05	0.5889	7.2361
SFN	98.36	8.0E-06	2.0254	8.6429
IFIT3	88.03	1.0E-05	5.6776	12.1344
EPSTI1	80.45	5.3E-05	0.4419	6.7726
FN1	77.71	0.0425	0.3713	6.6485
XAF1	73.52	5.1E-05	1.2037	7.4007
LDHA	70.03	0.0416	1.0524	7.1862
CMPK2	68.59	0.0003	0.0000	6.1050
LDLR	57.28	0.0001	0.5557	6.3936
CCL5	46.85	0.0330	0.0000	5.5507
MAP2	44.63	0.0120	0.0000	5.4776
LAMP3	41.64	0.0138	0.0000	5.3842
AKR1C2	39.95	3.7E-05	0.9960	6.3163
ULBP2	38.32	10.0E-06	2.5465	7.8047
IL6	37.01	0.0035	1.9557	7.1619
OAS3	35.51	6.8E-07	3.9936	9.1474
USP18	33.13	2.6E-06	3.2260	8.2809
TNFSF13B	32.90	3.2E-05	1.9315	6.9762

Table 2
Top 30 downregulated genes after MARV infection of primary PTC (40 h p.i.) (Ave. = average, q-value = FDR adjusted p-value).

Gene	Fold change	q-value	Ave. Mock	Ave. MARV
RPL14	−250.73	0.0405	10.2300	2.2578
SLC35B2	−60.97	0.0463	6.0883	0.1563
MATR3	−58.89	0.0298	6.0388	0.1571
DGUOK	−47.50	0.0283	5.8133	0.2465
SLC2A2	−45.57	9.3E-05	5.7007	0.1953
MC4R	−32.90	0.0009	5.2545	0.2103
LIMS1	−28.05	0.0408	4.8124	0.0000
SLC17A1	−21.86	0.0008	4.4546	0.0000
LYG1	−21.41	0.0053	6.3627	1.9427
CINP	−21.11	0.0143	4.3955	0.0000
RPLP2	−19.56	0.0213	8.3296	4.0366
NAXE	−18.90	0.0493	4.2439	0.0000
METTL17	−16.91	0.0446	4.9338	0.8543
SMYD3	−15.67	0.0248	4.7174	0.7471
SLC3A1	−15.14	0.0288	4.4820	0.5607
PADI2	−13.55	6.8E-07	8.5828	4.8259
F2RL1	−13.45	0.0288	3.9346	0.1806
OGDHL	−13.45	0.0364	5.5138	1.7642
MZT2B	−13.36	0.0488	6.5635	2.8274
RNF19A	−13.18	0.0487	4.6474	0.9264
MAP4K2	−12.82	0.0029	3.7724	0.0900
NAT8	−12.47	0.0394	3.9524	0.3158
TNFRSF6B	−10.93	0.0417	3.4513	0.0000
RPL3	−10.48	0.0252	10.2529	6.8655
PHLDB2	−9.38	0.0398	3.6617	0.4302
KCNIP1	−8.82	0.0295	4.5573	1.4185
CLSTN2	−8.63	5.3E-05	6.7249	3.6107
LAGE3	−8.00	0.0193	3.0029	0.0000
TMEM185A	−7.84	0.0368	2.9739	0.0000
PHB2	−7.52	0.0034	7.3486	4.4353

MARV-infected PTC, a gene ontology (GO) analysis was conducted using the Jensen COMPARTMENTS resource (Binder et al., 2014) (Fig. 2B, C). Here for upregulated transcripts an enrichment of the LPS receptor-, STING-, and interferon regulatory factor complexes (IRF-7 and IRF-3) were identified, among others (Fig. 2B). On the other hand, factors linked to ribosomes, the spindle checkpoint signaling (NDC80- and MAD1 complex), as well ribonucleoprotein complexes and mitochondria were identified among the downregulated transcripts, summarized in compartments analysis (Fig. 2C).

Taken together, the top upregulated genes and cellular compartments reveal a strong inflammatory and antiviral response, while some of the most-downregulated factors are involved in translation and cellular energy homeostasis.

3.3. The major biological themes in MARV-infected PTC

To define central biological themes in MARV-infected PTC the "Molecular Signatures Database" (MSigDB) Hallmark's gene sets were employed (Liberzon et al., 2011), allowing for an enrichment by highly refined gene data representing specific biological states (Liberzon et al., 2015). By utilizing UMAP (uniform manifold approximation and projection), a dimension reduction algorithm revealing the data's essential topological structure, changes in 20 prominent biological themes could be identified (Fig. 3A). Here a strong inflammatory response by interferon α, - *y* and TNFα signaling is confirmed and extended by analysis of the most strongly induced themes. In addition, prominent changes in cholesterol homeostasis, the complement system and apoptosis-related factors were obtained. In comparison, MYC- and EF2 targets, DNA repair, G2M checkpoint, and oxidative phosphorylation, as well as peroxisomes are prominent biological themes in the downregulated transcriptome (Fig. 3A).

Next, the examination of the enriched biological processes (Fig. 3C) demonstrated a strong regulation of viral genome replication, type I interferon response and regulation of IL-1ß secretion at 20 h p.i. In comparison, a response to type II interferon was detected for the first time at 40 h p.i. At this time point, also a strong downregulation of factors for RNA processing and translation, as well as SRP-dependent co-translational protein targeting to cell membranes are observed (Fig. 3C). Subsequently volcano plots were utilized to further illustrate the key biological themes (Figs. 4 and 5), thus allowing the strong interferon response to be analyzed in more detail (Fig. 4A). Besides the top upregulated transcripts from Table 1 (like RSAD2, OASL and CXCL10) the induction of inter alia CMPK2, EPSTI1 and USP18 was revealed, among others. In addition, a widespread and mostly upregulated alteration in cholesterol homeostasis was detected (Fig. 4C). Here, the most significant gene expression change was identified for SCD. The desaturase SCD plays a crucial role in the biosynthesis of monounsaturated fatty acids and aids in humoral immunity by supporting the mitochondrial metabolism of lymphocytes (Zhou et al., 2021). However, it should be noted that tubular cells also exhibit positive staining for SCD (Digre and Lindskog, 2020). Moreover, factors like IDI1 and FDFT1, both important enzymes in sterol biosynthesis, LDLR, the receptor involved in the uptake of LDL and triglyceride-rich lipoproteins, and STARD4, which is involved in cytosolic cholesterol transport, were also strongly upregulated (Fig. 4C). In contrast, factors relevant to oxidative phosphorylation are mainly downregulated at 40 h p.i., except for especially LDHA, which catalyzes the final step in anaerobic glycolysis. Among the downregulated gene sets are also MYC targets (Fig. 5A), members of the G2M checkpoint control (Fig. 5B) and a great number of spliceosome- as well as ribosome-related factors (Fig. 5C and D). The MYC data set demonstrates RPL14 as the strongest suppressed gene, but also includes factors like SRPK1 (regulating the localization of splicing factors), thus potentially linking MYC targets and regulation of splicing in MARV-infected PTC (Fig. 5A). The G2M checkpoint set (Fig. 5B) displays a majority of downregulated members, among them MYC and BIRC3 (also known as cellular inhibitor of apoptosis 2/cIAP2), who participates in NF-κB signaling and several forms of programmed cell death (Rodrigue-Gervais et al., 2014; Varfolomeev et al., 2008). Also, UBE2C - which is required for cell cycle progression (Hao et al., 2012) – and HMGN2 (associated with antiviral activity and open chromatin states

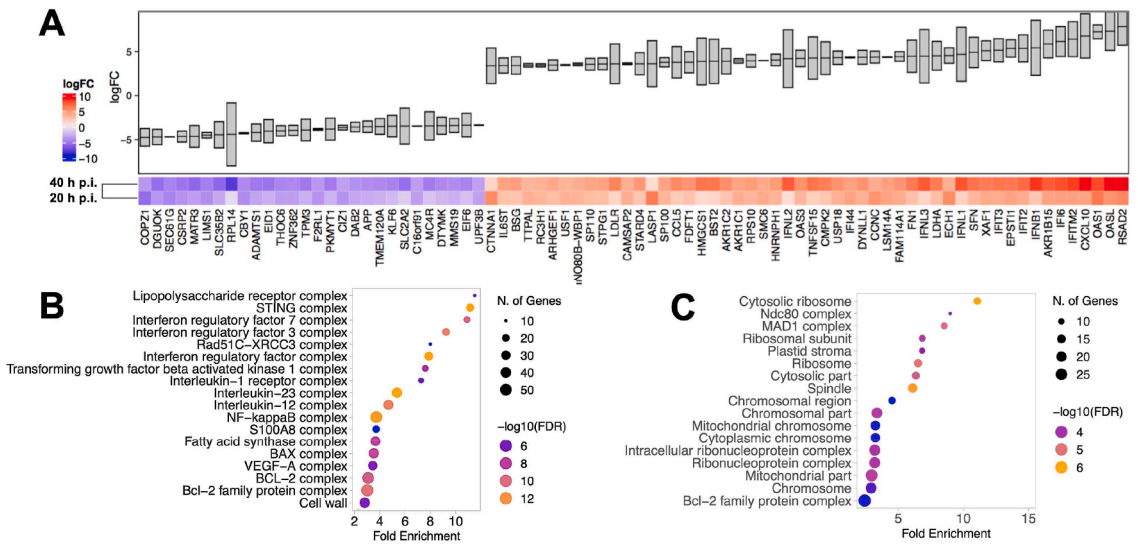

Fig. 2. Top up- and downregulated genes after MARV infection were investigated for enriched functional complexes and cellular compartments. (A) Top down- and upregulated genes at 20 h- and 40 h p.i. **(B)** GO analysis for enriched cellular compartments using the Jensen COMPARTMENTS database with up-regulated and **(C)** downregulated genes, both at 40 h p.i. (fold change cut-off ≥2 at an FDR = 0.05).

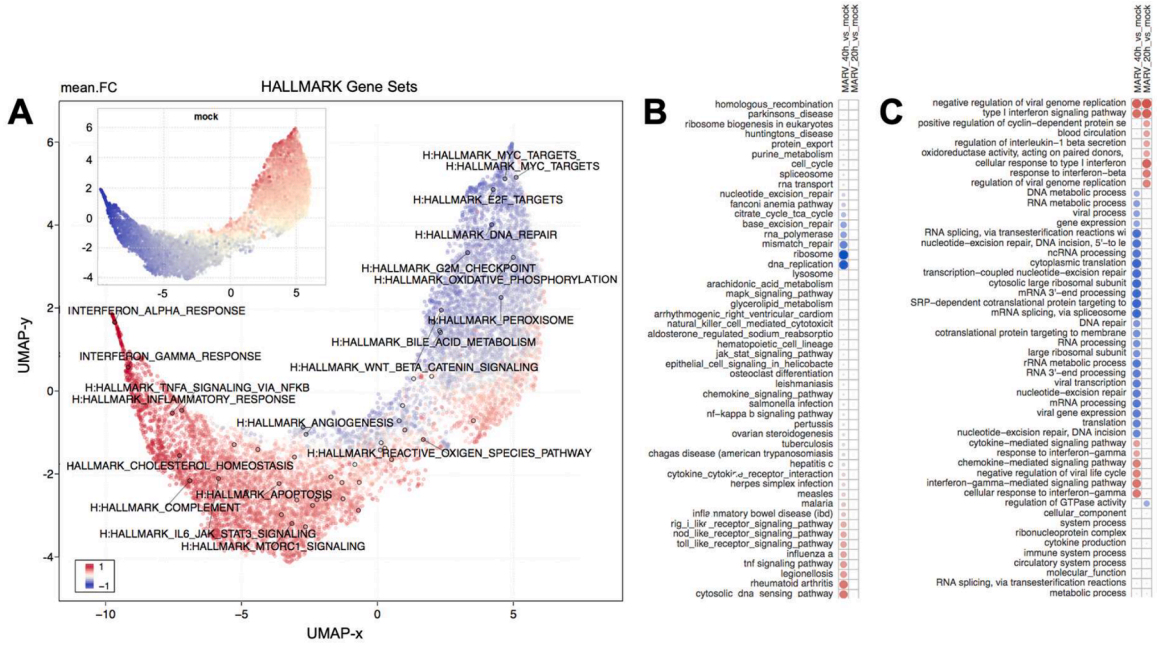

Fig. 3. UMAP clustering of gene sets and KEGG/GO activation heatmaps of MARV-infected PTC. (A) UMAP analysis of mock vs. MARV-infected PTC, displaying up- (red) and downregulated (blue) HALLMARK gene sets 40 h p.i. by mean of FC. The small square in the upper left of Fig. 1A represents the HALLMARK gene sets' state without MARV infection (mock replicates). The UMAP distance metric for Fig. 1A is covariance: gene sets that are clustered nearby have high covariance. Overall UMAP displays the data's essential topological structure. **(B)** KEGG activation heatmap 20 h and 40 h p.i. (upregulated processes are depicted in red, downregulated processes are shown in blue). **(C)** GO activation heatmap 20 h- and 40 h after MARV-infection (upregulated processes are depicted in red, downregulated processes are shown in blue).

(Feng et al., 2009; Paz and Ausió, 2016)), were found to be down-regulated in MARV-infected PTC. In contrast the GO spliceosome gene set (Fig. 5C) presents a more heterogeneous pattern, with down-regulated genes led by PABPC1 and SRFS1 compared to HNRNPH1 being the strongest upregulated member. In summary, UMAP and GO analyses as well as volcano plots demonstrate the mounting of an extensive interferon response, broad changes in cholesterol homeostasis, a downregulation of prominent factors in MYC target genes, and energy balance, among others.

3.4. *Network analysis reveals an energy-inflammation hub*

Based on experimentally established protein-protein interactions by STRING DB (Szklarczyk et al., 2018), PPARGC1A (PGC-1α) was identified as an energy-inflammation hub in MARV-infected PTC (Fig. 6). PGC-1α's primary interaction partners are displayed in Fig. 6A, indicating upregulated pro-inflammatory factors like IL6, TLR4 and TNF (TNFα) in contrast to downregulation of PGC-1α, MYC, APP and SLC2A2, among others. Considering the time kinetics (20 h- and 40 h p.i.) this response is increasing over time (Fig. 6C-F). PGC-1α is a known

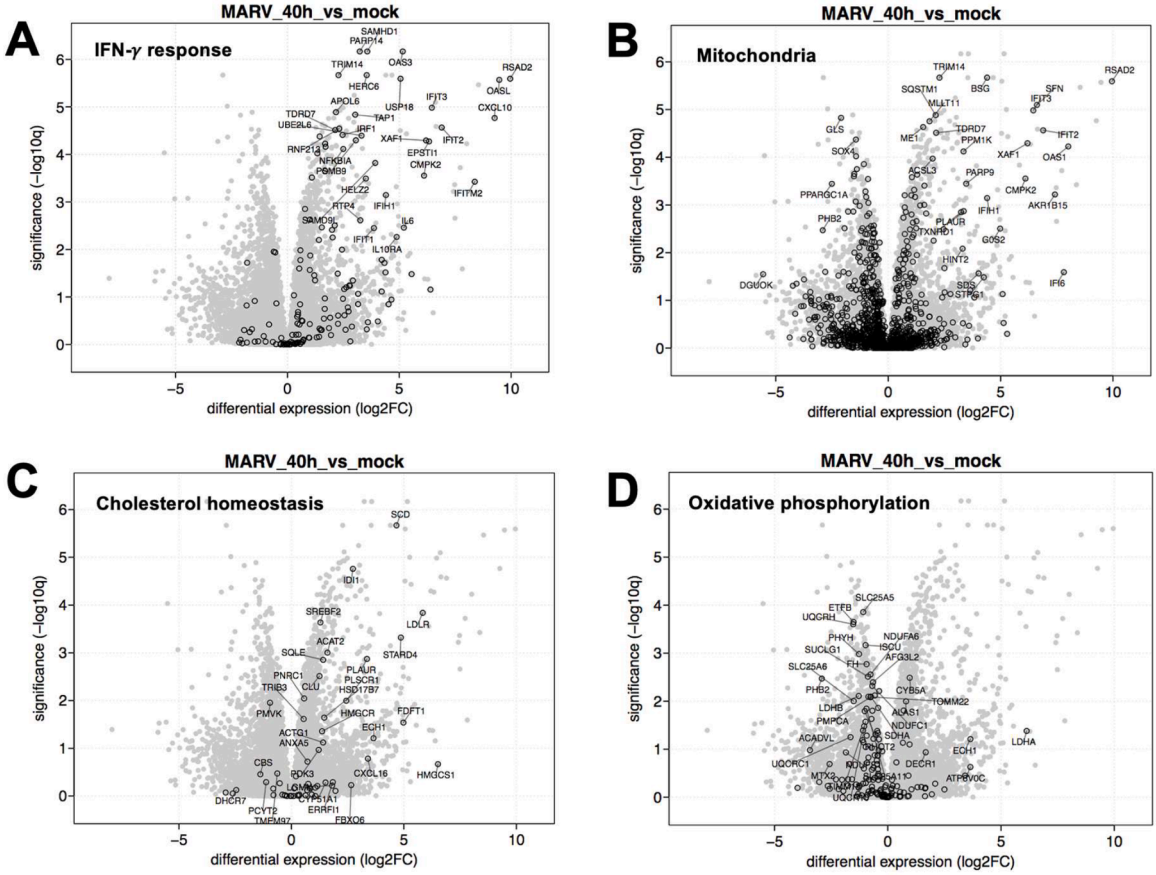

Fig. 4. Volcano plots of Hallmark/GO gene sets 40 h after MARV infection (log2FC vs. significance). (A) Hallmark IFN-$_\gamma$ response. **(B)** GO cellular component mitochondria. **(C)** Hallmark cholesterol homeostasis. **(D)** Hallmark oxidative phosphorylation.

master regulator of mitochondrial biogenesis, as well as gluconeogenesis (Rodgers et al., 2005). Moreover, PGC-1α interaction partners like the glucose transporter GLUT2 (coded for by SLC2A2) and the energy sensor NRF1 (coded by NFE2L1 (Qiu et al., 2022)), as well as ACADVL (catalyzing the first step of mitochondrial beta-oxidation (Aoyama et al., 1995), were found to be downregulated. Interestingly, the interferon signaling members STAT2, and IFITM3, were inversely correlated to PGC-1α (Fig. 6C and D), among others. Furthermore, factors crucial for cellular energy homeostasis like ENHO (coding for Adropin (Ali et al., 2022)), and MC4R (Krashes et al., 2016) were detected to be inversely correlated to a pro-inflammatory cytokine/antiviral response (Fig. 6E and F). The downregulation of PGC-1α was confirmed by RT-qPCR, revealing a more than 90 % reduction at 40 h p.i. compared to mock (Fig. 6G).

4. Discussion

In this study, we demonstrate an inflammation-induced altered PTC energy homeostasis as a potential factor for the clinically observed AKI in MVD. To date, there are no large-scale gene expression data on MARV-infected renal cell types, as clinical and pathological data on MVD are still scarce. However, autopsies in MVD patients have shown acute tubular insufficiency with predominant damage to proximal but not to distal tubular cells (Gear et al., 1975; Gedigk et al., 1968; Rippey et al., 1984). Also, MARV virions were detected by electron microscopy in renal tissue, as well as MARV antigen in PTC (Zaki and Goldsmith, 1999). In addition, live virus has been isolated from kidney tissue, as well as from urine (Martini and Siegert, 1971; Smith et al., 1982).

Clinically, AKI can be divided into three main causes: prerenal conditions (e.g., volume loss, shock, myocardial failure), intrarenal pathologies (capillary-, glomerular- or tubular dysfunction) and postrenal obstruction (Kellum et al., 2021; Thadhani et al., 1996). Viruses can cause prerenal or intrarenal AKI or a mixture thereof, as well as rarely postrenal AKI (Ban et al., 2022; Prasad and Patel, 2018; Rahman et al., 2012). In terms of prerenal causes, bleeding or gastrointestinal infection can result in relevant volume loss, but also infection of endothelial cells or hypercytokinemia may lead to capillary leakage, hypotension, and therefore insufficient renal blood flow and AKI. Yet, in Ebola virus (EBOV) infection, AKI developed before the prerenal stage (Hunt et al., 2015). This suggests an additional factor in the pathogenesis of filovirus AKI. Looking at the intrarenal situation, immunopathological effects, but also direct infection of glomerular and tubular cells has been reported for many viruses, inducing pathological changes of varying severity (Prasad and Patel, 2018). Virus-induced immune phenomena like acute glomerulonephritis are seen in infections with e.g., hepatitis viruses (A, B and C), herpes viruses (CMV, EBV), HIV or adenoviruses, among others (Wenderfer, 2015). In contrast, some viruses are known to directly infect renal (glomerular and/or tubular) cells. Prominent members are hantaviruses (causing hantavirus hemorrhagic fever with renal syndrome), Dengue virus (DENV), Zika virus (ZIKV), SARS-CoV-2 or Influenza A (IAV). Hantavirus-induced AKI is mainly associated to infection of endothelial cells, tubulointerstitial nephritis and dysregulated cytokine release (Krautkrämer et al., 2013; Mir, 2022). The pathophysiology of DENV-associated AKI is seen in dysregulated cytokine release and primarily glomerular injury (Bignardi et al., 2022; Lima et al., 2007). On the contrary, renal epithelial cells infected with ZIKV exhibit NLRP3 inflammasome activation (Chen et al., 2017; Liu et al., 2019). In IAV-associated AKI, acute tubular necrosis of distal tubular cells (DTC) and viral antigen in DTC and glomerular cells have been demonstrated during several pandemics (Beswick and Finlayson,

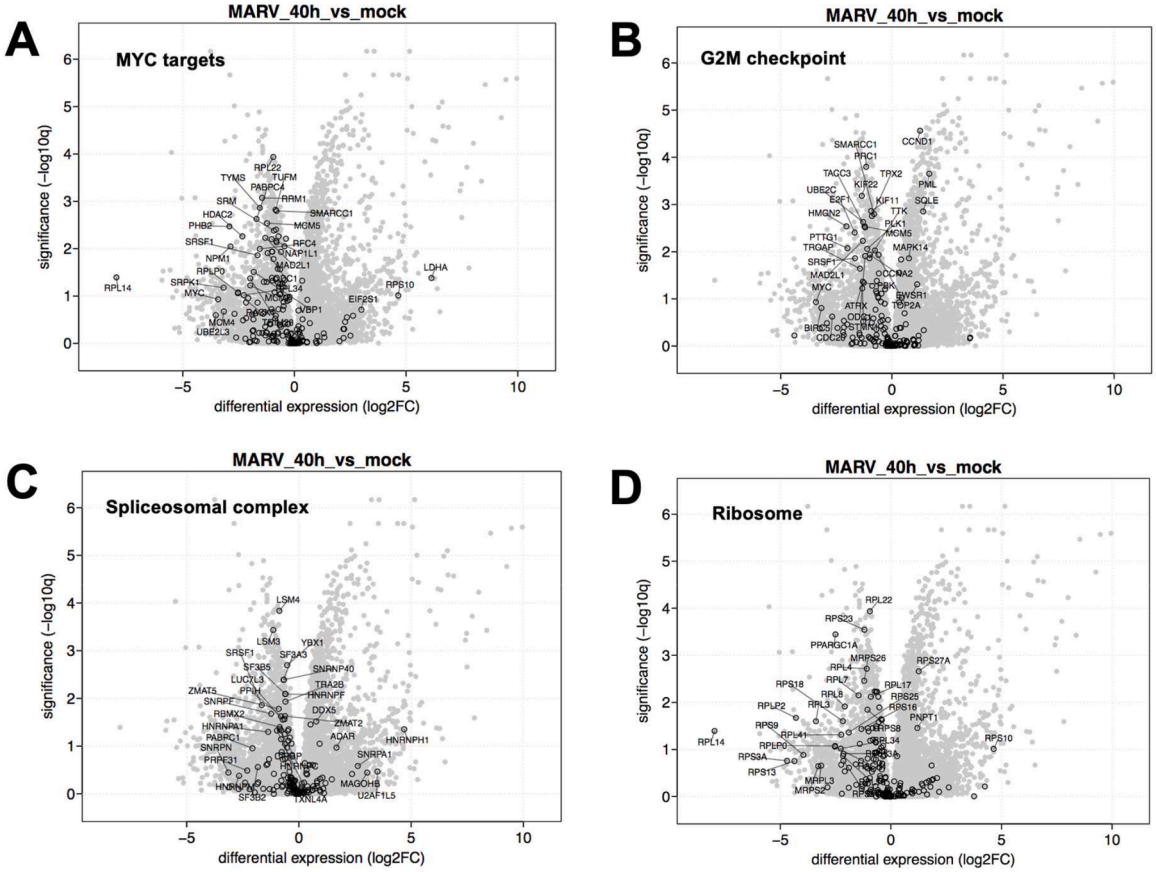

Fig. 5. Volcano plots of Hallmark/GO gene sets 40 h after MARV-infection (log2FC vs. significance). **(A)** Hallmark MYC targets. **(B)** Hallmark G2M checkpoint. **(C)** Hallmark spliceosomal complex. **(D)** GO cellular component ribosome.

1959; Nin et al., 2011; Zinserling et al., 1983). In COVID-19 patients, AKI was associated with hypoxia, heart failure, venous congestion, inflammation, and immune-mediated thrombosis, but also direct infection of renal cells (Legrand et al., 2021). Interestingly, proteomics of SARS-CoV-2-infected PTC revealed a strong interferon response and significant changes to the pathways linked to kidney injury (Kohli et al., 2022). Also, sequencing of single PTCs from COVID-19 AKI patients revealed an increase in pathways involved in apoptosis, response to reactive oxygen species and DNA repair (Cheung et al., 2021). However, the downregulation of energy-related factors in PTC has not been described in any of these viruses.

We show MARV infection and replication in primary human PTC, yet we did not observe a relevant CPE at multiple time points (20 h- and 40 h p.i.). This is consistent with some available MVD autopsies, where visible pathological changes in individual organs were generally not severe enough to explain the fatal outcome of the disease (Olinger et al., 2010). However, our transcriptome analyses revealed a profound inflammatory and antiviral response by IFNα, -γ and TNFα signaling in contrast to substantial downregulation of key cellular energy factors. While a strong inflammatory response by interferon-response genes has been reported for MARV and Ebola virus (EBOV) in human whole blood samples (Speranza et al., 2020), assessment of filovirus-induced shifts in cellular energy states have not been reported in human cells yet. Interestingly, a downregulation of mitochondrial biogenesis and PGC-1α is induced in DENV-infected liver cells (Singh et al., 2022). Under physiological conditions, PTCs require a constant supply of energy for active transport processes, particularly those involved in water and electrolyte balance, amino acid and glucose re-uptake, and detoxification (Bhargava and Schnellmann, 2017). These energy-intensive apical (towards the tubular lumen) and basolateral (towards the capillaries) tasks are fueled by pre-dominantly citrate cycle intermediates (Brinkkoetter et al., 2019). Consequently, the main energy supply in PTC is by oxidative phosphorylation (OXPHOS). To these aims fatty acids, amino acids and lactate provide metabolites for the PTC's citrate cycle (Schaub et al., 2021; Singh, 2023). We found mRNA for PGC-1α, a key factor in mitochondrial biogenesis, as well as lipid and glucose metabolism (Bhargava and Schnellmann, 2017; Lee et al., 2019; Rodgers et al., 2005), to be substantially downregulated in MARV-infected PTC. Although up to now not investigated in viral infections of renal cells, PGC-1α is known as an important factor in septic AKI (Stallons et al., 2013). In PTC, PGC-1α was suppressed in response to TNFα or endotoxemia, and a PTC-specific gene depletion of PGC-1α led to persistent kidney injury in knockout mice (Tran et al., 2011). Critically, maladaptation after AKI may be responsible for fibrosis and chronic kidney disease (CKD), as CKD patient samples show downregulation of key enzymes in fatty acid oxidation and lipid accumulation in the diseased kidney, led by downregulation of the PPARA-PGC-1α axis (Kang et al., 2015). In addition to PTC, cardiac and skeletal tissues also show inflammation-induced changes in cellular energy states: in cardiomyocytes, TNFα induces PGC-1α repression through interaction with the p65 subunit of NF-κB (Álvarez-Guardia et al., 2010). Pro-inflammatory NF-κB signaling also causes the downregulation of PGC-1α, -fatty acid oxidation and ATP synthesis in skeletal muscle cells (Nisr et al., 2019). PGC-1α is also known to control metabolic adaptation required for host defence in rhinovirus-infected airway epithelial cells: PGC-1α upregulation by pharmacological induction restored epithelial barrier function, reduced disease severity, and enhanced viral defence (Michi et al., 2021). In addition to PGC-1α, other noteworthy factors in energy homeostasis such as ENHO, MC4R, GLUT2, and NRF1 (which is targeted by PGC-1α (Wu et al., 1999)), were also downregulated in our experiment. Notably,

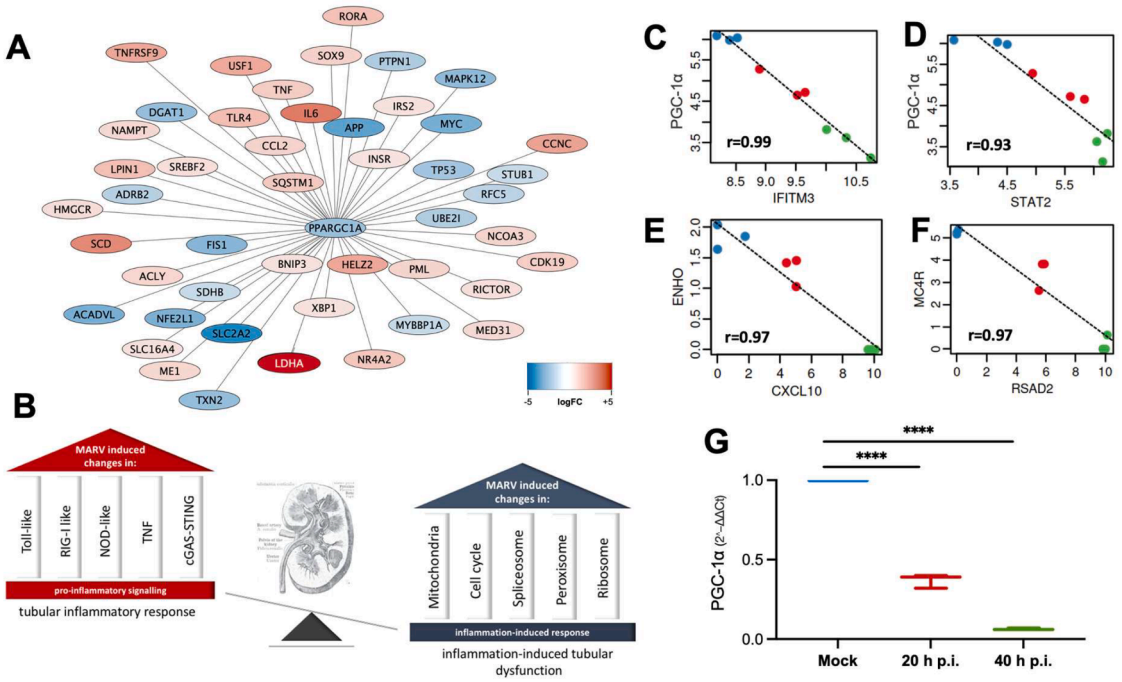

Fig. 6. Inflammation-induced changes in key cellular energy players in MARV-infected PTC. (A) Network analysis of shared up- and downregulated genes 20 h- and 40 h after MARV infection (upregulated genes are depicted in red, downregulated genes are shown in blue (PPARGC1A = PGC-1α). **(B)** Summary of PTC inflammatory response pathways vs. inflammation-induced tubular dysfunction upon MARV infection. **(C)** Correlation analysis PGC-1α vs. IFITM3 (blue depicts mock, red 20 h p.i. and green replicates at 40 h p.i. Data are based on RNAseq CPM (counts per million). **(D)** Correlation analysis PGC-1α vs. TRIM21 (data based on CPM). **(E)** Correlation analysis ENHO vs. CXCL10 (data based on CPM). **(F)** Correlation analysis MC4R vs. RSAD2 (data based on CPM). **(G)** PGC-1α expression changes after MARV-infection (2ˆ−ΔΔCt, as verified by RT-qPCR).

we discovered an inverse correlation of the forementioned factors to interferon-response genes like IFITM3, STAT2 or RSAD2, thus implicating a potential AKI-relevance in other virus-induced diseases. While the alterations induced by MARV in the energy supply of PTC are likely to be a significant contributing factor to AKI in MVD, it is important to note that there are various other changes revealed in the transcriptome data, e.g., the top downregulated factor in our analysis, RPL14. RPL14, a part of the large 60S ribosomal subunit, has been identified as direct target of viral proteins (e.g., hepatitis C virus (HCV), dengue virus) and is known to be also downregulated in influenza A-, respiratory syncytial virus -or coronavirus infections; nevertheless, the precise role of RPL14 remains undefined (Cervantes-Salazar et al., 2015; Emmott et al., 2013; Lee et al., 2011; Zhu and Xin, 2015). Moreover, other top down-regulated transcripts were those from CMPK2, EPSTI1, and USP18. CMPK2 is known to be important for antiviral cytokine release and mitochondrial response in dengue virus infection (Lai et al., 2021), while overexpression of EPSTI1 is reported to effectively inhibit HCV replication (Meng et al., 2015). USP18 is involved in dampening the interferon response by cleaving ISG15-ubiquitin conjugates and, importantly USP18 -/- mice have been reported to be resistant to otherwise fatal viral infections (Ritchie et al., 2004). Therefore, it is conceivable, that MARV inhibits viral clearance in PTC on multiple levels.

However, this study has certain limitations. As we aimed to closely replicate the human environment, our primary experiments were conducted using human cells instead of mouse or non-human primate cells. Therefore, we simulated the epithelial aspect of a human tubule to MARV infection, yet the effects of MARV-infection on other renal cell types apart from PTC should be investigated in an organ context (e.g. organoids or 3D co-cultures), as this will assist in comprehending other effects of virus replication, as well as cellular effects. For further and comprehensive analysis in an outbreak setting, where kidney biopsies pose a risk in unstable or bleeding patients, the non-invasive investigation of AKI pathophysiology by urinary single-cell sequencing could prove to be an important alternative (Klocke et al., 2022). Furthermore, MARV's subversion of the innate and adaptive immune response (Fernando et al., 2015; Fritz et al., 2008; Mohamadzadeh et al., 2006) cannot be reflected by our *in vitro* PTC model. Certainly, our transcriptome results need further analysis and evaluation of protein levels to strengthen the hypothesis that MARV modulate energy supply of PTC.

5. Conclusion

Taken together, transcriptome analysis of MARV-infected primary human PTC reveals the picture of strong tubular inflammatory response and significant reactive changes in tubular energy metabolism as a possible contributing factor in MARV-associated AKI.

Funding

The research was funded in part by University Hospital Frankfurt am Main (B.K., H.G., P.C.B.), the German Center for Infection Research (DZIF) (O.D.) as well as by the Deutsche Forschungsgemeinschaft (DFG, German Research Foundation) SFB 1021 (O.D.).

The study was conducted in accordance with the Declaration of Helsinki and approved by the ethics committee of the clinic of the Goethe University, Frankfurt (UGO 03/10, Amendment, 05 Dec 2014).

Informed consent was obtained from all subjects involved in the study.

The data presented in this study are openly available in NCBI GEO at https://www.ncbi.nlm.nih.gov/geo/query/acc.cgi?acc=GSE226148.

CRediT authorship contribution statement

Benjamin Koch: Writing – original draft, Visualization,

Investigation, Funding acquisition, Formal analysis, Conceptualization. **Maximilian Filzmayer:** Writing – original draft, Investigation, Formal analysis. **Sammy Patyna:** Writing – original draft. **Nils Wetzstein:** Writing – original draft. **Sebastian Lampe:** Writing – original draft, Investigation. **Tobias Schmid:** Writing – original draft, Resources. **Helmut Geiger:** Writing – original draft, Resources. **Patrick C. Baer:** Writing – original draft, Resources, Methodology. **Olga Dolnik:** Writing – original draft, Visualization, Supervision, Resources, Methodology, Investigation, Funding acquisition, Formal analysis, Conceptualization.

Declaration of competing interest

The authors declare that they have no known competing financial interests or personal relationships that could have appeared to influence the work reported in this paper.

Data availability

The data presented in this study are openly available in NCBI GEO GSE226148.

Acknowledgments

We thank Rita Schmitt-Prokopp and Professor Dr. Michael Lein (Department of Urology, Sana Hospital, Offenbach, Germany) for providing human kidney tissue. We are also grateful to Dr. Nelly Mostajo for valuable discussions. The authors thank Professor Dr. Stephan Becker, Dr. Markus Eickmann and the BSL-4 technical team for the opportunity to perform the BSL-4 experiments in the BSL-4 laboratory at the Philipps University of Marburg.

Supplementary materials

Supplementary material associated with this article can be found, in the online version, at doi:10.1016/j.virusres.2024.199337.

References

Akhmedov, M., Martinelli, A., Geiger, R., Kwee, I., 2019. Omics playground: a comprehensive self-service platform for visualization, analytics and exploration of big omics data. NAR. Genom. Bioinform. 2, lqz019. https://doi.org/10.1093/nargab/lqz019.

Ali, I.I., D'Souza, C., Singh, J., Adeghate, E., 2022. Adropin's role in energy homeostasis and metabolic disorders. Int. J. Mol. Sci. 23, 8318. https://doi.org/10.3390/ijms23158318.

Álvarez-Guardia, D., Palomer, X., Coll, T., Davidson, M.M., Chan, T.O., Feldman, A.M., Laguna, J.C., Vázquez-Carrera, M., 2010. The p65 subunit of NF-κB binds to PGC-1α, linking inflammation and metabolic disturbances in cardiac cells. Cardiovasc. Res. 87, 449–458. https://doi.org/10.1093/cvr/cvq080.

Amman, B.R., Carroll, S.A., Reed, Z.D., Sealy, T.K., Balinandi, S., Swanepoel, R., Kemp, A., Erickson, B.R., Comer, J.A., Campbell, S., Cannon, D.L., Khristova, M.L., Atimnedi, P., Paddock, C.D., Crockett, R.J.K., Flietstra, T.D., Warfield, K.L., Unfer, R., Katongole-Mbidde, E., Downing, R., Tappero, J.W., Zaki, S.R., Rollin, P.E., Ksiazek, T.G., Nichol, S.T., Towner, J.S., 2012. Seasonal pulses of Marburg virus circulation in juvenile rousettus aegyptiacus bats coincide with periods of increased risk of human infection. PLoS Pathog. 8, e1002877 https://doi.org/10.1371/journal.ppat.1002877.

Aoyama, T., Souri, M., Ueno, I., Kamijo, T., Yamaguchi, S., Rhead, W.J., Tanaka, K., Hashimoto, T., 1995. Cloning of human very-long-chain acyl-coenzyme A dehydrogenase and molecular characterization of its deficiency in two patients. Am. J. Hum. Genet. 57, 273–283.

Baer, P.C., Hahn, J.B., Schubert, R., Geiger, H., 2006. Differentiation status of human renal proximal and distal tubular epithelial cells *in vitro*: differential expression of characteristic markers. Cells Tissues. Organs 184, 16–22. https://doi.org/10.1159/000096947.

Baer, P.C., Nockher, W.A., Haase, W., Scherberich, J.E., 1997. Isolation of proximal and distal tubule cells from human kidney by immunomagnetic separation: technical Note. Kidney Int. 52, 1321–1331. https://doi.org/10.1038/ki.1997.457.

Ban, H., Miura, K., Tomoeda, R., Hirai, K., Hattori, M., 2022. Acute kidney injury due to ammonium acid urate stones in a patient with adenovirus gastroenteritis: a case report. BMC Urol. 22, 5. https://doi.org/10.1186/s12894-022-00954-4.

Banerjee, A., Vest, K.E., Pavlath, G.K., Corbett, A.H., 2017. Nuclear poly(A) binding protein 1 (PABPN1) and Matrin3 interact in muscle cells and regulate RNA processing. Nucleic Acids Res. 45 https://doi.org/10.1093/nar/gkx786 gkx786-.

Bente, D., Gren, J., Feldmann, H., 2009. Disease modeling for ebola and Marburg viruses. Dis. Model. Mech. 2, 12–17. https://doi.org/10.1242/dmm.000471.

Beswick, I.P., Finlayson, R., 1959. A renal lesion in association with Influenza. J. Clin. Pathol. 12, 280. https://doi.org/10.1136/jcp.12.3.280.

Bhargava, P., Schnellmann, R.G., 2017. Mitochondrial energetics in the kidney. Nat. Rev. Nephrol. 13, 629–646. https://doi.org/10.1038/nrneph.2017.107.

Bignardi, P.R., Pinto, G.R., Boscarioli, M.L.N., Lima, R.A.A., Delfino, V.D.A., 2022. Acute kidney injury associated with dengue virus infection: a review. Braz. J. Nephrol. 44, 232–237. https://doi.org/10.1590/2175-8239-jbn-2021-0221.

Binder, J.X., Pletscher-Frankild, S., Tsafou, K., Stolte, C., O'Donoghue, S.I., Schneider, R., Jensen, L.J., 2014. Compartments: unification and visualization of protein subcellular localization evidence. Database. https://doi.org/10.1093/database/bau012 bau012.

Bolger, A.M., Lohse, M., Usadel, B., 2014. Trimmomatic: a flexible trimmer for Illumina sequence data. Bioinformatics. 30, 2114–2120. https://doi.org/10.1093/bioinformatics/btu170.

Brauburger, K., Hume, A.J., Mühlberger, E., Olejnik, J., 2012. Forty-five years of Marburg virus research. Viruses 4, 1878–1927. https://doi.org/10.3390/v4101878.

Bray, N.L., Pimentel, H., Melsted, P., Pachter, L., 2016. Near-optimal probabilistic RNA-seq quantification. Nat. Biotechnol. 34, 525–527. https://doi.org/10.1038/nbt.3519.

Brinkkoetter, P.T., Bork, T., Salou, S., Liang, W., Mizi, A., Özel, C., Koehler, S., Hagmann, H.H., Ising, C., Kuczkowski, A., Schnyder, S., Abed, A., Schermer, B., Benzing, T., Kretz, O., Puelles, V.G., Lagies, S., Schlimpert, M., Kammerer, B., Handschin, C., Schell, C., Huber, T.B., 2019. Anaerobic glycolysis maintains the glomerular filtration barrier independent of mitochondrial metabolism and dynamics. Cell Rep. 27, 1551–1566. https://doi.org/10.1016/j.celrep.2019.04.012.

Cervantes-Salazar, M., Angel-Ambrocio, A.H., Soto-Acosta, R., Bautista-Carbajal, P., Hurtado-Monzon, A.M., Alcaraz-Estrada, S.L., Ludert, J.E., Angel, R.M.D., 2015. Dengue virus NS1 protein interacts with the ribosomal protein RPL18: this interaction is required for viral translation and replication in Huh-7 cells. Virology 484, 113–126. https://doi.org/10.1016/j.virol.2015.05.017.

Chen, Jian, Yang, Y.F., Chen, Jun, Zhou, X., Dong, Z., Chen, T., Yang, Y., Zou, P., Jiang, B., Hu, Y., Lu, L., Zhang, X., Liu, J., Xu, J., Zhu, T., 2017. Zika virus infects renal proximal tubular epithelial cells with prolonged persistency and cytopathic effects. Emerg. Microbes Infec. 6, e77. https://doi.org/10.1038/emi.2017.67.

Cheung, M.D., Erman, E.N., Liu, S., Erdmann, N.B., Ghajar-Rahimi, G., Moore, K.H., Edberg, J.C., George, J.F., Agarwal, A., 2021. Single-cell RNA sequencing of urinary cells reveals distinct cellular diversity in COVID-19-associated AKI. Kidney 360 (3), 28–36. https://doi.org/10.34067/kid.0005522021.

de la Ritchie, K.J., Hahn, C.S., Kim, K.I., Yan, M., Rosario, D., Li, L., Torre, J.C., Zhang, D. E., 2004. Role of ISG15 protease UBP43 (USP18) in innate immunity to viral infection. Nat. Med. 10, 1374–1378. https://doi.org/10.1038/nm1133.

Digre, A., Lindskog, C., 2020. The Human Protein Atlas—Spatial localization of the human proteome in health and disease. Protein Sci. 30, 218–233. https://doi.org/10.1002/pro.3987.

Dolnik, O., Kolesnikova, L., Becker, S., 2008. Filoviruses: interactions with the host cell. Cell Mol. Life Sci. 65, 756–776. https://doi.org/10.1007/s00018-007-7406-2.

Emmott, E., Munday, D., Bickerton, E., Britton, P., Rodgers, M.A., Whitehouse, A., Zhou, E.M., Hiscox, J.A., 2013. The cellular interactome of the coronavirus infectious bronchitis virus nucleocapsid protein and functional implications for virus biology. J. Virol. 87, 9486–9500. https://doi.org/10.1128/jvi.00321-13.

Fang, R., Jiang, Q., Guan, Y., Gao, P., Zhang, R., Zhao, Z., Jiang, Z., 2021. Golgi apparatus-synthesized sulfated glycosaminoglycans mediate polymerization and activation of the cGAMP sensor STING. Immunity 54, 962–975. https://doi.org/10.1016/j.immuni.2021.03.011.

Feldmann, Knipe, D.M., Howley, P.M., 2013. Fields Virology, 6th ed. LWW. p. 923ff.

Feng, Y., He, F., Zhang, P., Wu, Q., Huang, N., Tang, H., Kong, X., Li, Y., Lu, J., Chen, Q., Wang, B., 2009. Inhibitory effect of HMGN2 protein on human hepatitis B virus expression and replication in the HepG2.2.15 cell line. Antivir. Res. 81, 277–282. https://doi.org/10.1016/j.antiviral.2008.12.011.

Fernando, L., Qiu, X., Melito, P.L., Williams, K.J.N., Feldmann, F., Feldmann, H., Jones, S.M., Alimonti, J.B., 2015. Immune response to marburg virus angola infection in nonhuman primates. J. Infect. Dis. 212, S234–S241. https://doi.org/10.1093/infdis/jiv095.

Fritz, E.A., Geisbert, J.B., Geisbert, T.W., Hensley, L.E., Reed, D.S., 2008. Cellular immune response to marburg virus infection in cynomolgus macaques. Viral. Immunol. 21, 355–364. https://doi.org/10.1089/vim.2008.0023.

Ge, S.X., Jung, D., Yao, R., 2019. ShinyGO: a graphical gene-set enrichment tool for animals and plants. Bioinformatics 36, 2628–2629. https://doi.org/10.1093/bioinformatics/btz931.

Ge, S.X., Son, E.W., Yao, R., 2018. iDEP: an integrated web application for differential expression and pathway analysis of RNA-Seq data. BMC Bioinform. 19, 534. https://doi.org/10.1186/s12859-018-2486-6.

Gear, J.S., Cassel, G.A., Gear, A.J., Trappler, B., Clausen, L., Meyers, A.M., Kew, M.C., Bothwell, T.H., Sher, R., Miller, G.B., Schneider, J., Koornhof, H.J., Gomperts, E.D., Isaäcson, M., Gear, J.H., 1975. Outbreake of Marburg virus disease in Johannesburg. Brit. Med. J. 4, 489. https://doi.org/10.1136/bmj.4.5995.489.

Gedigk, P., Bechtelsheimer, H., Korb, G., 1968. Die pathologische Anatomie der „Marburg-Virus"-Krankheit (sog. „Marburger Affenkrankheit"). Dtsch. Med. Wochenschr. 93, 590–601. https://doi.org/10.1055/s-0028-1105101.

Hao, Z., Zhang, H., Cowell, J., 2012. Ubiquitin-conjugating enzyme UBE2C: molecular biology, role in tumorigenesis, and potential as a biomarker. Tumor Biol. 33, 723–730. https://doi.org/10.1007/s13277-011-0291-1.

Hunt, L., Gupta-Wright, A., Simms, V., Tamba, F., Knott, V., Tamba, K., Heisenberg-Mansaray, S., Tamba, E., Sheriff, A., Conteh, S., Smith, T., Tobin, S., Brooks, T., Houlihan, C., Cummings, R., Fletcher, T., 2015. Clinical presentation, biochemical, and haematological parameters and their association with outcome in patients with Ebola virus disease: an observational cohort study. Lancet Infect. Dis. 15, 1292–1299. https://doi.org/10.1016/s1473-3099(15)00144-9.

Kang, H.M., Ahn, S.H., Choi, P., Ko, Y.A., Han, S.H., Chinga, F., Park, A.S.D., Tao, J., Sharma, K., Pullman, J., Bottinger, E.P., Goldberg, I.J., Susztak, K., 2015. Defective fatty acid oxidation in renal tubular epithelial cells has a key role in kidney fibrosis development. Nat. Med. 21, 37–46. https://doi.org/10.1038/nm.3762.

Kellum J.A., Romagnani P., Ashuntantang G., Ronco C., Zarbock A., Anders H.J., 2021. Acute kidney injury. Nat Rev Dis Primers 7, 52. 10.1038/s41572-021-00284-z.

Klocke, J., Kim, S.J., Skopnik, C.M., Hinze, C., Boltengagen, A., Metzke, D., Grothgar, E., Prskalo, L., Wagner, L., Freund, P., Görlich, N., Muench, F., Schmidt-Ott, K.M., Mashreghi, M.F., Kocks, C., Eckardt, K.U., Rajewsky, N., Enghard, P., 2022. Urinary single-cell sequencing captures kidney injury and repair processes in human acute kidney injury. Kidney Int. 102, 1359–1370. https://doi.org/10.1016/j.kint.2022.07.032.

Kohli, A., Sauerhering, L., Fehling, S.K., Klann, K., Geiger, H., Becker, S., Koch, B., Baer, P.C., Strecker, T., Münch, C., 2022. Proteomic landscape of SARS-CoV-2– and MERS-CoV–infected primary human renal epithelial cells. Life Sci. Alliance 5, e202201371. https://doi.org/10.26508/lsa.202201371.

Krashes, M.J., Lowell, B.B., Garfield, A.S., 2016. Melanocortin-4 receptor–regulated energy homeostasis. Nat. Neurosci. 19, 206–219. https://doi.org/10.1038/nn.4202.

Krautkrämer, E., Zeier, M., Plyusnin, A., 2013. Hantavirus infection: an emerging infectious disease causing acute renal failure. Kidney Int. 83, 23–27. https://doi.org/10.1038/ki.2012.360.

Lai, J.H., Wu, D.W., Wu, C.H., Hung, L.F., Huang, C.Y., Ka, S.M., Chen, A., Chang, Z.F., Ho, L.J., 2021. Mitochondrial CMPK2 mediates immunomodulatory and antiviral activities through IFN-dependent and IFN-independent pathways. iScience 24, 102498. https://doi.org/10.1016/j.isci.2021.102498.

Lee, G., Uddin, M.J., Kim, Y., Ko, M., Yu, I., Ha, H., 2019. PGC-1α, a potential therapeutic target against kidney aging. Aging Cell 18, e12994. https://doi.org/10.1111/acel.12994.

Lee, J.W., Liao, P.C., Young, K.C., Chang, C.L., Chen, S.S.L., Chang, T.T., Lai, M.D., Wang, S.W., 2011. Identification of hnRNPH1, NF45, and C14orf166 as novel host interacting partners of the mature hepatitis C virus core protein. J. Proteome Res. 10, 4522–4534. https://doi.org/10.1021/pr200338d.

Legrand, M., Bell, S., Forni, L., Joannidis, M., Koyner, J.L., Liu, K., Cantaluppi, V., 2021. Pathophysiology of COVID-19-associated acute kidney injury. Nat. Rev. Nephrol. 1–14. https://doi.org/10.1038/s41581-021-00452-0.

Liberzon, A., Birger, C., Thorvaldsdóttir, H., Ghandi, M., Mesirov, J.P., Tamayo, P., 2015. The molecular signatures database hallmark gene set collection. Cell Syst. 1, 417–425. https://doi.org/10.1016/j.cels.2015.12.004.

Liberzon, A., Subramanian, A., Pinchback, R., Thorvaldsdóttir, H., Tamayo, P., Mesirov, J.P., 2011. Molecular signatures database (MSigDB) 3.0. Bioinformatics 27, 1739–1740. https://doi.org/10.1093/bioinformatics/btr260.

Ligon, B.L., 2005. Outbreak of marburg hemorrhagic fever in angola: a review of the history of the disease and its biological aspects. Semin. Pediatr. Infect. Dis. 16, 219–224. https://doi.org/10.1053/j.spid.2005.05.001.

Lima, E.Q., Gorayeb, F.S., Zanon, J.R., Nogueira, M.L., Ramalho, H.J., Burdmann, E.A., 2007. Dengue haemorrhagic fever-induced acute kidney injury without hypotension, haemolysis or rhabdomyolysis. Nephrol. Dial. Transplant. 22, 3322–3326. https://doi.org/10.1093/ndt/gfm431.

Liu, T., Tang, L., Tang, H., Pu, J., Gong, S., Fang, D., Zhang, H., Li, Y.P., Zhu, X., Wang, W., Wu, M., Liao, Y., Li, C., Zhou, H., Huang, X., 2019. Zika virus infection induces acute kidney injury through activating NLRP3 inflammasome via suppressing Bcl-2. Front. Immunol. 10, 1925. https://doi.org/10.3389/fimmu.2019.01925.

Martines, R.B., Ng, D.L., Greer, P.W., Rollin, P.E., Zaki, S.R., 2015. Tissue and cellular tropism, pathology and pathogenesis of Ebola and Marburg viruses. J Pathology 235, 153–174. https://doi.org/10.1002/path.4456.

Martini, G.A., Siegert, R., 1971. Marburg Virus Disease. Springer Science & Business Media. https://doi.org/10.1007/978-3-662-01593-3.

McInnes, L., Healy, J., Melville, J., 2018. UMAP: uniform manifold approximation and projection for dimension reduction. In: J. Open Source Softw., 3, p. 861. https://doi.org/10.21105/joss.00861.

Mehedi, M., Falzarano, D., Seebach, J., Hu, X., Carpenter, M.S., Schnittler, H.J., Feldmann, H., 2011. A new ebola virus nonstructural glycoprotein expressed through RNA editing. J. Virol. 85, 5406–5414. https://doi.org/10.1128/jvi.02190-10.

Meng, X., Yang, D., Yu, R., Zhu, H., 2015. EPSTI1 is involved in IL-28A-mediated inhibition of HCV infection. Mediat. Inflamm. 716315 https://doi.org/10.1155/2015/716315.

Michi, A.N., Yipp, B.G., Dufour, A., Lopes, F., Proud, D., 2021. PGC-1α mediates a metabolic host defense response in human airway epithelium during rhinovirus infections. Nat. Commun. 12, 3669. https://doi.org/10.1038/s41467-021-23925-z.

Mir, S., 2022. Hantavirus Induced Kidney Disease. Front. Med. 8, 795340 https://doi.org/10.3389/fmed.2021.795340.

Mohamadzadeh, D.M., Chen, L., Olinger, G.G., Pratt, W.D., Schmaljohn, A.L., 2006. Filoviruses and the balance of innate, adaptive, and inflammatory responses. Viral Immunol. 19, 602–612. https://doi.org/10.1089/vim.2006.19.602.

Morchikh, M., Cribier, A., Raffel, R., Amraoui, S., Cau, J., Severac, D., Dubois, E., Schwartz, O., Bennasser, Y., Benkirane, M., 2017. HEXIM1 and NEAT1 long non-coding RNA form a multi-subunit complex that regulates DNA-mediated innate Immune response. Mol. Cell 67, 387–399. https://doi.org/10.1016/j.molcel.2017.06.020 e5.

Nin, N., Lorente, J.A., Sánchez-Rodríguez, C., Granados, R., Ver, L.S., Soto, L., Hidalgo, J., Fernández-Segoviano, P., Ortín, J., Esteban, A., 2011. Kidney histopathological findings in fatal pandemic 2009 influenza A (H1N1). Intensive Care Med. 37, 880–881. https://doi.org/10.1007/s00134-011-2183-7.

Nisr, R.B., Shah, D.S., Ganley, I.G., Hundal, H.S., 2019. Proinflammatory NFkB signalling promotes mitochondrial dysfunction in skeletal muscle in response to cellular fuel overloading. Cell Mol. Life Sci. 76, 4887–4904. https://doi.org/10.1007/s00018-019-03148-8.

Olinger, Mahy, B.W.J., Regenmortel, M.H.V., et al., 2010. Desk Encyclopedia of Human and Medical Virology. Academic Press., p. 391ff.

Paassen, J.van, Bauer, M.P., Arbous, M.S., Visser, L.G., Schmidt-Chanasit, J., Schilling, S., Ölschläger, S., Rieger, T., Emmerich, P., Schmetz, C., Berkmortel, F.van de, Hoek, B. van, Burgel, N.D.van, Osterhaus, A.D., Vossen, A.C., Günther, S., Dissel, J.T.van, 2012. Acute liver failure, multiorgan failure, cerebral oedema, and activation of proangiogenic and antiangiogenic factors in a case of Marburg haemorrhagic fever. Lancet Infect. Dis. 12, 635–642. https://doi.org/10.1016/s1473-3099(12)70018-x.

Paz, A.M.de, Ausió, J., 2016. HMGNs: the enhancer charmers. Bioessays 38, 226–231. https://doi.org/10.1002/bies.201500157.

Pfaffl, M.W., 2001. A new mathematical model for relative quantification in real-time RT-PCR. Nucleic Acids Res. 29, e45. https://doi.org/10.1093/nar/29.9.e45.

Poliquin, G., Funk, D., Jones, S., Tran, K., Ranadheera, C., Hagan, M., Tierney, K., Grolla, A., Dhaliwal, A., Bello, A., Leung, A., Nakamura, C., Kobasa, D., Falzarano, D., Garnett, L., Bovendo, H.F., Feldmann, H., Kesselman, M., Hansen, G., Gren, J., Risi, G., Biondi, M., Mortimer, T., Racine, T., Deschambault, Y., Aminian, S., Edmonds, J., Sourette, R., Allan, M., Rondeau, L., Hadder, S., Press, C., DeGraff, C., Kucas, S., Cook, B.W.M., Hancock, B.J., Kumar, A., Soni, R., Schantz, D., McKitrick, J., Warner, B., Griffin, B.D., Qiu, X., Kobinger, G.P., Safronetz, D., Stein, D., Cutts, T., Kenny, J., Soule, G., Kozak, R., Theriault, S., Menec, L., Vendramelli, R., Higgins, S., Liu, G., Rahim, N.M., Kasloff, S., Sloan, A., He, S., Tailor, N., Gray, M., Strong, J.E., 2019. Impact of intensive care unit supportive care on the physiology of Ebola virus disease in a universally lethal non-human primate model. Intensive Care Med. Exp. 7, 54. https://doi.org/10.1186/s40635-019-0268-8.

Prasad, A.N., Ronk, A.J., Widen, S.G., Wood, T.G., Basler, C.F., Bukreyev, A., 2020. Ebola virus produces discrete small noncoding RNAs independently of the host microRNA pathway which lack RNA interference activity in bat and human cells. J. Virol. 94, e01441–19. https://doi.org/10.1128/jvi.01441-19.

Prasad, N., Patel, M.R., 2018. Infection-induced kidney diseases. Front. Med. 5, 327. https://doi.org/10.3389/fmed.2018.00327.

Qiu, L., Yang, Q., Zhao, W., Xing, Y., Li, P., Zhou, X., Ning, H., Shi, R., Gou, S., Chen, Y., Zhai, W., Wu, Y., Li, G., Chen, Z., Ren, Y., Gao, Y., Zhang, Y., Qi, Y., 2022. Dysfunction of the energy sensor NFE2L1 triggers uncontrollable AMPK signaling and glucose metabolism reprogramming. Cell Death Dis. 13, 501. https://doi.org/10.1038/s41419-022-04917-3.

Rahman, M., Shad, F., Smith, M.C., 2012. Acute kidney injury: a guide to diagnosis and management. Am. Fam. Physician 86, 631–639.

Rippey, J.J., Schepers, N.J., Gear, J.H.S., 1984. The pathology of Marburg virus disease. South Afr. Med. J. 66, 50–54.

Rodgers, J.T., Lerin, C., Haas, W., Gygi, S.P., Spiegelman, B.M., Puigserver, P., 2005. Nutrient control of glucose homeostasis through a complex of PGC-1α and SIRT1. Nature 434, 113–118. https://doi.org/10.1038/nature03354.

Rodrigue-Gervais, I.G., Labbé, K., Dagenais, M., Dupaul-Chicoine, J., Champagne, C., Morizot, A., Skeldon, A., Brincks, E.L., Vidal, S.M., Griffith, T.S., Saleh, M., 2014. Cellular inhibitor of apoptosis protein cIAP2 protects against pulmonary tissue necrosis during influenza virus infection to promote host survival. Cell Host. Microbe 15, 23–35. https://doi.org/10.1016/j.chom.2013.12.003.

Rougeron, V., Feldmann, H., Grard, G., Becker, S., Leroy, E.M., 2015. Ebola and Marburg haemorrhagic fever. J. Clin. Virol. 64, 111–119. https://doi.org/10.1016/j.jcv.2015.01.014.

Schaub, J.A., Venkatachalam, M.A., Weinberg, J.M., 2021. Proximal tubular oxidative metabolism in acute kidney injury and the transition to CKD. Kidney360 2, 355–364. https://doi.org/10.34067/kid.0004772020.

Shannon, P., Markiel, A., Ozier, O., Baliga, N.S., Wang, J.T., Ramage, D., Amin, N., Schwikowski, B., Ideker, T., 2003. Cytoscape: a software environment for integrated models of biomolecular interaction networks. Genome Res. 13, 2498–2504. https://doi.org/10.1101/gr.1239303.

Singh, P., 2023. Reprogramming of energy metabolism in kidney disease. Nephron. 147, 61–64. https://doi.org/10.1159/000526308.

Singh, B., Avula, K., Sufi, S.A., Parwin, N., Das, S., Alam, M.F., Samantaray, S., Bankapalli, L., Rani, A., Poornima, K., Prusty, B., Mallick, T.P., Shaw, S.K., Dodia, H., Kabi, S., Pagad, T.T., Mohanty, S., Syed, G.H., 2022. Defective mitochondrial quality control during dengue infection contributes to disease pathogenesis. J. Virol. 96, e00828. https://doi.org/10.1128/jvi.00828-22.

Smith, D.H., Isaacson, M., Johnson, K.M., Bagshawe, A., Johnson, B.K., Swanapoel, R., Killey, M., Siongok, T., Keruga, W.K., 1982. Marburg virus disease in Kenya. Lancet 319, 816–820. https://doi.org/10.1016/s0140-6736(82)91871-2.

Speranza, E., Caballero, I., Honko, A.N., Johnson, J.C., Bohannon, J.K., DeWald, L.E., Gerhardt, D.M., Sword, J., Hensley, L.E., Bennett, R.S., Connor, J.H., 2020. Previremic identification of ebola or marburg virus infection using integrated host-transcriptome and viral genome detection. mBio 11, e01157. https://doi.org/10.1128/mbio.01157-20.

Stallons, L.J., Funk, J.A., Schnellmann, R.G., 2013. Mitochondrial homeostasis in acute organ failure. Curr. Pathobiol. Rep. 1, 169–177. https://doi.org/10.1007/s40139-013-0023-x.

Stille, W., Böhle, E., Martini, G.A., Siegert, R., 1971. Marburg virus disease. Springer 10–18. https://doi.org/10.1007/978-3-662-01593-3_2.

Szklarczyk, D., Gable, A.L., Lyon, D., Junge, A., Wyder, S., Huerta-Cepas, J., Simonovic, M., Doncheva, N.T., Morris, J.H., Bork, P., Jensen, L.J., von Mering, C., 2018. STRING v11: protein–protein association networks with increased coverage, supporting functional discovery in genome-wide experimental datasets. Nucleic Acids Res. 47, gky1131. https://doi.org/10.1093/nar/gky1131.

Thadhani, R., Pascual, M., Bonventre, J.V., 1996. Acute renal failure. New Engl. J. Med. 334, 1448–1460. https://doi.org/10.1056/nejm199605303342207.

Tran, M., Tam, D., Bardia, A., Bhasin, M., Rowe, G.C., Kher, A., Zsengeller, Z.K., Akhavan-Sharif, M.R., Khankin, E.V., Saintgeniez, M., David, S., Burstein, D., Karumanchi, S.A., Stillman, I.E., Arany, Z., Parikh, S.M., 2011. PGC-1α promotes recovery after acute kidney injury during systemic inflammation in mice. J. Clin. Invest. 121, 4003–4014. https://doi.org/10.1172/jci58662.

Varfolomeev, E., Goncharov, T., Fedorova, A.V., Dynek, J.N., Zobel, K., Deshayes, K., Fairbrother, W.J., Vucic, D., 2008. c-IAP1 and c-IAP2 are critical mediators of tumor necrosis factor α (TNFα)-induced NF-κB Activation. J. Biol. Chem. 283, 24295–24299. https://doi.org/10.1074/jbc.c800128200.

von Mering, C., Huynen, M., Jaeggi, D., Schmidt, S., Bork, P., Snel, B., 2003. STRING: a database of predicted functional associations between proteins. Nucleic Acids Res. 31, 258–261. https://doi.org/10.1093/nar/gkg034.

Wenderfer, S.E., 2015. Viral-associated glomerulopathies in children. Pediatr. Nephrol. 30, 1929–1938. https://doi.org/10.1007/s00467-015-3057-y.

Wu, Z., Puigserver, P., Andersson, U., Zhang, C., Adelmant, G., Mootha, V., Troy, A., Cinti, S., Lowell, B., Scarpulla, R.C., Spiegelman, B.M., 1999. Mechanisms controlling mitochondrial biogenesis and respiration through the thermogenic coactivator PGC-1. Cell 98, 115–124. https://doi.org/10.1016/s0092-8674(00)80611-x.

Zaki, S.R., Goldsmith, C.S., 1999. Pathologic features of filovirus infections in humans. Curr. Top. Microbiol. Immunol. 235, 97–116.

Zhou, X., Zhu, X., Li, C., Li, Y., Ye, Z., Shapiro, V.S., Copland, J.A., Hitosugi, T., Bernlohr, D.A., Sun, J., Zeng, H., 2021. Stearoyl-CoA desaturase-mediated monounsaturated fatty acid availability supports humoral immunity. Cell Rep. 34, 108601 https://doi.org/10.1016/j.celrep.2020.108601.

Zhu, H., Xin, X., 2015. Common dysregulation of ribosomal genes present in infants with acute respiratory infection of respiratory syncytial virus, rhinovirus, and influenza A. Pediatr. Allergy Immunol. Pulmonol. 28, 32–40. https://doi.org/10.1089/ped.2014.0400.

Zinserling, V.A., Aksenov, O.A., Melnikova, V.F., Zinserling, V.A., 1983. Extrapulmonary lesions in influenza. Tohoku J. Exp. Med. 140, 259–272. https://doi.org/10.1620/tjem.140.259.